Lyapunov Analysis of Two Imbalanced Power System Areas

Gilang Nugraha Putu Pratama[1†] and **Adha Imam Cahyadi**[2], Non-members

ABSTRACT

Transient stability refers to the system's capability to preserve synchronism while affected by large disturbances. It is a nonlinear problem that requires the simultaneous solution of many differential equations. Therefore, a thorough analysis is needed to resolve it. In this paper, we present an analysis of multimachine transient stability under different fault cases using the Lyapunov function. It serves as an analytical tool to determine the condition necessary for stability. The system remains stable as long as it is contained in the region of attraction. Meanwhile, the swing equation and reduced admittance matrix are used to model the system in three conditions: pre-fault, during the fault, and post-fault. Numerical simulations are conducted to verify the preservation of synchronism under fault on the transmission lines by achieving the critical clearing time.

Keywords: Lyapunov Function, Multimachine, Power System Stability, Transient Stability, Critical Clearing Time

1. INTRODUCTION

Over the years, power system stability has become a major concern [1]. It can be classified into rotor angle, frequency, and voltage stability as illustrated in Fig. 1.

Power system stability is a nonlinear problem that requires the simultaneous solution of many differential equations [2]. Operating conditions can be distinguished into steady-state and transient stability. Steady-state stability denotes the capability of the power system functioning during operation despite being under small disturbances [3]. Meanwhile, transient stability is required to deal with large disturbances while preserving the synchronism [4]. Practically, transient stability is the main issue in most systems [5] since a sudden loss in generation is likely to cause a power outage [6].

Meanwhile, the loss of load or fault in transmission facilities may disrupt stability on a smaller scale. The responses to such disturbances involve large excursions of rotor angles and are affected by the nonlinear power-angle relationship. Stability depends on the initial condition of the system and severity of the disturbance [7]. Most of the time, systems are altered after the disturbance takes place, leading them to operate in different conditions from their initial state. These states can be asserted as pre-fault, fault, and post-fault conditions.

In this paper, the different conditions of the faults affecting the transient stability of the system are investigated. The severity and location of the faults have different impacts on the network, and rigorous work is required to anticipate these scenarios. Therefore, numerical simulation is utilized in order to gain better insight and tackle the problem. The data and parameters obtained from the simulation can be used to determine the transient stability and optimal system conditions [8–11].

Two significant parameters determine the stability of a system: fault clearing time and critical clearing time. As its name suggests, the fault clearing time (FCT) is the time at which the fault is cleared. Meanwhile, the critical clearing time (CCT) is the FCT at which the system remains at a stable level. The system is unstable if the FCT is greater than the CCT. Alternatively, if the FCT is less or equal to the CCT, then the system is stable [12].

Some related works are worthy of mention here. Previously, Simulink, Demiroren, and Zeynelgil prevailed in simulating the transient stability of a single-machine infinite bus [13]. Despite the model being oversimplified, it serves its purpose well. In another work by Dadashzadeh and Sanaye-Pasand [14], transient stability was successfully simulated, although there was no further discussion on the FCT and CCT.

Here, several fault scenarios are taken into consideration to evaluate the stability of the FCT and CCT. Moreover, the stability analysis using the Lyapunov function is presented here. The remainder of this paper is set out as follows. The necessary equations are discussed in Section 2, while the numerical simulations and analysis are presented in Section 3, elaborating on the construction of the

Manuscript received on October 3, 2020 ; revised on July 3, 2021 ; accepted on July 6, 2021. This paper was recommended by Associate Editor Kaan Kerdchuen.

[1]The author is with the Department of Electronics and Informatics Engineering Education, Universitas Negeri Yogyakarta, Indonesia.

[2]The author is with the Department of Electrical Engineering and Information Technology, Universitas Gadjah Mada, Indonesia.

[†]Corresponding author: gilang.n.p.pratama@uny.ac.id

Digital Object Identifier 10.37936/ecti-eec.2021193.242123

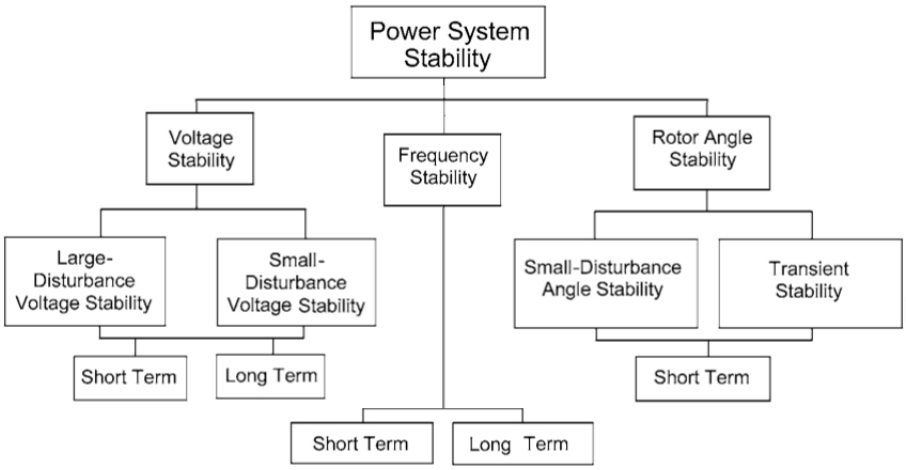

Fig. 1: *Classification of power system stability.*

Table 1: *List of symbols.*

Symbols	Notes
P_m	Mechanical power input
P_e	Electrical power output
M	Inertia constant
E	Internal voltage of the machine
D	Damping constant
$\mathbf{Y}$	The $m \times m$ admittance matrix
$\mathbf{Y}_{red}$	The $n \times n$ reduced admittance matrix
$\mathbf{Y}_A$	The $n \times n$ submatrix
$\mathbf{Y}_B$	The $n \times r$ submatrix
$\mathbf{Y}_C$	The $r \times n$ submatrix
$\mathbf{Y}_D$	The $r \times r$ submatrix
δ	Rotor angle
ω	Angular velocity
G	Transfer conductance
B	Transfer susceptance

Lyapunov function and the stability region. Lastly, the conclusion of this paper can be found in Section 4.

2. SYSTEM EQUATIONS

In this section, mathematical expressions are used to present the system model. Some symbols are briefly explained in Table 1 to ease the understanding of equations.

Let us assert here that n and m represent the number of machines and the entire nodes in the network, while r is the number of nodes in the network excluding the machines. The generating station and transmission line are represented briefly in Fig. 2.

2.1 Nodal Equation

The admittance matrix is required to obtain the currents delivered to the network [15]. It can be calculated using the nodal equation. Assuming m number of nodes, the nodal equation can be expressed as follows

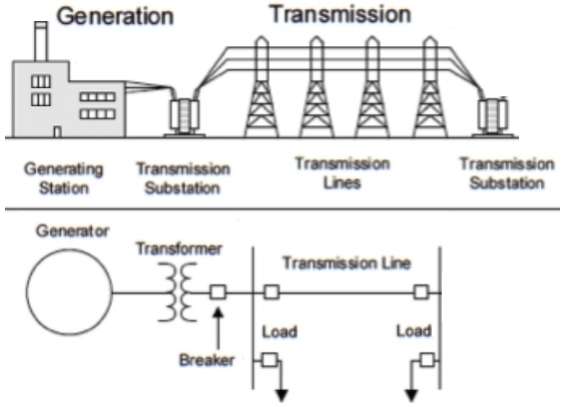

Fig. 2: *Generation unit and transmission line.*

$$\begin{bmatrix} I_1 \\ \vdots \\ I_n \\ 0 \\ \vdots \\ 0 \end{bmatrix} = \mathbf{Y} \begin{bmatrix} E_1 \\ \vdots \\ E_n \\ E_{n+1} \\ \vdots \\ E_m \end{bmatrix} \tag{1}$$

where $I_1, \ldots, I_n$ are the currents injected from the machines, while the other nodes have zero injection currents. Accordingly, Eq. (1) can be rewritten into a more concise form as

$$\begin{bmatrix} \mathbf{I_n} \\ \mathbf{Z_r} \end{bmatrix} = \mathbf{Y} \begin{bmatrix} \mathbf{E_n} \\ \mathbf{E_r} \end{bmatrix} \tag{2}$$

where, $\mathbf{I_n}$ and $\mathbf{Z_r}$ are the injected current and zero column vector, respectively, while the column vectors $\mathbf{E_n}$ and $\mathbf{E_r}$ are the internal voltage of the generator and the potential drop between nodes, respectively. The admittance matrix is $m \times m$ matrix, which can be partitioned as

$$\mathbf{Y} = \left[\begin{array}{c|c} \mathbf{Y}_{\mathrm{A}} & \mathbf{Y}_{\mathrm{B}} \\ \hline \mathbf{Y}_{\mathrm{C}} & \mathbf{Y}_{\mathrm{D}} \end{array}\right]. \tag{3}$$

According to Eqs. (2) and (3), these conditions hold

$$\mathbf{I_n} = \mathbf{Y}_{\mathrm{A}}\mathbf{E_n} + \mathbf{Y}_{\mathrm{B}}\mathbf{E_r} \tag{4}$$

$$\mathbf{Z_r} = \mathbf{Y}_{\mathrm{C}}\mathbf{E_n} + \mathbf{Y}_{\mathrm{D}}\mathbf{E_r}. \tag{5}$$

Furthermore, the potential drop between nodes $\mathbf{E_r}$, can be ignored [15] and denoted as

$$\mathbf{I_n} = \mathbf{Y}_{\mathrm{red}}\mathbf{E_n}. \tag{6}$$

The reduced admittance matrix can be obtained by performing the matrix operation since all the nodes are considered to have zero injection currents except for those in the internal generator [9]. Therefore, the admittance matrix can be reduced as

$$\mathbf{Y}_{\mathrm{red}} = \mathbf{Y}_{\mathrm{A}} - \mathbf{Y}_{\mathrm{B}}\mathbf{Y}_{\mathrm{D}}^{-\mathbf{1}}\mathbf{Y}_{\mathrm{C}}. \tag{7}$$

Since there are n number of machines, the reduced admittance matrix can be expressed as

$$\mathbf{Y}_{\mathrm{red}} = \begin{bmatrix} \bar{\mathrm{Y}}_{11} & \dots & \bar{\mathrm{Y}}_{1n} \\ \vdots & \ddots & \vdots \\ \bar{\mathrm{Y}}_{n1} & \dots & \bar{\mathrm{Y}}_{nn} \end{bmatrix} \tag{8}$$

Technically, the admittance matrix can be composed of diagonal and off-diagonal elements. First, let us denote the diagonal elements as

$$\bar{\mathrm{Y}}_{ii} = \mathrm{Y}_{\mathrm{ii}}\angle\theta_{\mathrm{ii}} = \mathrm{G}_{\mathrm{ii}} + \mathrm{iB}_{\mathrm{ii}} \tag{9}$$

representing the driving admittance of the i^{th} machine. Meanwhile, the off-diagonal elements,

$$\bar{\mathrm{Y}}_{ij} = \mathrm{Y}_{\mathrm{ij}}\angle\theta_{\mathrm{ij}} = \mathrm{G}_{\mathrm{ij}} + \mathrm{iB}_{\mathrm{ij}} \tag{10}$$

represent the admittance between nodes i^{th} to j^{th} . The reduced admittance matrix in Eq. (7) serves as a convenient analytical method. It can be used to represent the condition of transmission lines in pre-fault, during the fault, and post-fault. Nevertheless, it is viable if the loads are assumed to be constant impedances [15].

2.2 Swing Equation

Some assumptions are made to simplify the model and satisfy the purposes [15–18]. In this paper, we make the following assumptions.

1. The flux linkages are constant during the transient period.
2. The mechanical power input, $\mathrm{P_m}$, is constant.
3. The loads are constant impedances.

Most of the time, the first assumption is valid, since the flux decay is much slower than the transient phenomena [16]. In general, the order of the governed time is higher than the transient periods. Therefore, the second assumption is valid for transient studies [17]. Arguably, the last assumption provides the simplest nontrivial load model, yet is quite reliable [15, 18].

Based on these assumptions, the swing equation can be denoted as

$$\mathrm{M_i}\ddot{\delta}_{\mathrm{i}} + \mathrm{D_i}\dot{\delta}_{\mathrm{i}} = \mathrm{P_{mi}} - \mathrm{P_{ei}} \tag{11}$$

where $i = 1, \dots, n$ representing the machine indices. Regarding the swing equation above, these states hold

$$\omega_i = \dot{\delta}_i \tag{12}$$

$$\dot{\omega}_i = -\frac{\mathrm{D_i}}{\mathrm{M_i}}\omega_i + \mathrm{P_{mi}} - \mathrm{P_{ei}}. \tag{13}$$

The electrical power output can be denoted as

$$\mathrm{P_{ei}} = \mathrm{E_i^2 G_{ii}} + \sum_{\substack{j=1 \\ j\neq i}}^{\mathrm{n}} \mathrm{E_i E_j Y_{ij}} \cos\left(\theta_{\mathrm{ij}} - \delta_{\mathrm{i}} + \delta_{\mathrm{j}}\right). \tag{14}$$

3. LYAPUNOV STABILITY ANALYSIS AND CASE STUDIES

This section presents the stability analysis, conducted using the Lyapunov function, along with the case studies. It is necessary to construct a valid Lyapunov function, which can subsequently be used to determine the stability region of the system. Meanwhile, the case studies are carried out by performing numerical simulation using MATLAB/Simulink.

Two cases are presented here. In the first case, we consider the fault on the transmission lines through which the current is unlikely to flow. Obviously, the remaining line needs to retain connection to both power areas. The unbalanced load between the two areas is then presented in the second case study. Whether or not the synchronism can be preserved is verified in both case studies by numerical simulation. It is worth mentioning here, that the non-uniform damping constants are utilized in both cases.

3.1 Construction of Lyapunov Function

The stability analysis employs Lyapunov's direct method. It is rather philosophical, yet a useful analytical tool which follows the concept of energy [19]. Assuming $\mathcal{E}(x)$ is the energy function of an isolated system and $\dot{\mathcal{E}}(x)$ the rate of change. Since $\dot{\mathcal{E}}(x)$ should be negative, the energy will decrease gradually. It continues until the energy function reaches its minimum, such as $\mathcal{E}(x_0)$, where in this case $x_0 = 0$. The energy function $\mathcal{E}(x)$ can be redefined as the Lyapunov function $\mathcal{V}(x)$ which is more convenient for applications. The system is stable if a positive definite Lyapunov function $\mathcal{V}(x)$

exists, whereas its derivative $\dot{\mathcal{V}}(x)$ is a negative semidefinite.

Unfortunately, there is no such canonical method for constructing the Lyapunov function. Here, we utilize a method proposed by Moore and Anderson, which considers a generalized Popov criterion requiring the equation to be represented in a state-space form [20]. Furthermore, it applies zero transfer conductance.

Usually, the transfer conductance is neglected for practicality [16, 17]. Therefore, Eq. (14) can be rewritten as

$$\mathrm{P_{ei}} = \mathrm{E_i^2 G_{ii}} + \sum_{\substack{j=1 \\ j \neq i}}^{2} \mathrm{E_i E_j B_{ij}} \sin\left(\delta_\mathrm{i} - \delta_\mathrm{j}\right) \tag{15}$$

where the equilibrium states are $\mathrm{P_{ei}} = \mathrm{P_{mi}}$, $\omega_i = 0$, and the equilibrium load angles are δ_1° and δ_2°. Hence, the equilibrium states can be denoted as

$$\sum_{i=1}^{2} \mathrm{P_{mi}} = \sum_{\mathrm{i}=1}^{2} \mathrm{E_i^2 G_{ii}}. \tag{16}$$

After asserting the equilibrium states, the state-space can be defined due to Willems in the form of Luré [16], such as

$$\dot{\mathbf{x}} = \mathbf{A}\mathbf{x} - \mathbf{B}\mathbf{f}\left(\sigma\right) \tag{17}$$

$$\sigma = \mathbf{C}\mathbf{x} \tag{18}$$

where the state vector $\mathbf{x} = \begin{bmatrix} \boldsymbol{\omega}^\mathsf{T} & \boldsymbol{\delta}^\mathsf{T} \end{bmatrix}^\mathsf{T}$, is a 4×1 column vector. It consists of 2×1 column vectors, such as $\boldsymbol{\omega} = \begin{bmatrix} \omega_1 & \omega_2 \end{bmatrix}^\mathsf{T}$ and $\boldsymbol{\delta} = \begin{bmatrix} \delta_1 - \delta_1^\circ & \delta_2 - \delta_2^\circ \end{bmatrix}^\mathsf{T}$.

The matrices are as follows

$$\mathbf{A} = \begin{bmatrix} -\mathbf{D}\mathbf{M}^{-\mathbf{1}} & \mathbf{Z_{2\times 2}} \\ \mathbf{I_{2\times 2}} & \mathbf{Z_{2\times 2}} \end{bmatrix} \tag{19}$$

$$\mathbf{B} = \begin{bmatrix} \mathbf{M}^{-\mathbf{1}}\mathbf{K} \\ \mathbf{Z_{2\times 1}} \end{bmatrix} \tag{20}$$

$$\mathbf{C} = \begin{bmatrix} \mathbf{Z_{1\times 2}} & \mathbf{K}^\mathsf{T} \end{bmatrix} \tag{21}$$

where the vector $\mathbf{K} = \begin{bmatrix} 1 & -1 \end{bmatrix}^\mathsf{T}$, the diagonal matrix $\mathbf{D} = \mathrm{diag}\{\mathrm{D_1}, \mathrm{D_2}\}$, and the diagonal matrix $\mathbf{M} = \mathrm{diag}\{\mathrm{M_1}, \mathrm{M_2}\}$. As previously mentioned, the function $f\left(\sigma\right)$ can be defined as

$$f\left(\sigma\right) = \mathrm{E_1 E_2 Y_{12}}\{\sin\left(\xi - \xi^\circ\right) - \sin\left(\xi^\circ\right)\} \tag{22}$$

where $\xi = \left(\delta_1 - \delta_1^\circ\right) - \left(\delta_2 - \delta_2^\circ\right)$ and $\xi^\circ = \delta_1^\circ - \delta_2^\circ$. After explaining the essentials, we can outline the Moore-Anderson formalism to determine the Lyapunov function. Let a positive real matrix be

$$\mathbf{W} = \left(\alpha + \beta\mathbf{s}\right)\mathbf{C}\left(\mathbf{s}\mathbf{I_{2\times 2}} - \mathbf{A}\right)^{-\mathbf{1}}\mathbf{B} \tag{23}$$

where α and β are two real numbers and $\mathbf{P}$ also exists as an arbitrary positive definite symmetric matrix, which satisfies these conditions

$$\mathbf{P}\mathbf{A} + \mathbf{A}^\mathsf{T}\mathbf{P} = -\mathbf{L}\mathbf{L}^\mathsf{T} \tag{24}$$

$$\mathbf{P}\mathbf{B} = \alpha\mathbf{C}^\mathsf{T} + \beta\mathbf{A}^\mathsf{T}\mathbf{C}^\mathsf{T} - \gamma\mathbf{L} \tag{25}$$

$$\gamma^2 = \beta\mathbf{C}\mathbf{B} + \beta\mathbf{B}^\mathsf{T}\mathbf{C}^\mathsf{T} \tag{26}$$

where $\mathbf{L}$ is an auxiliary square matrix. Proof of these conditions is provided by Anderson [21].

On the other hand, since $\mathbf{C}\mathbf{B} = \mathbf{B}^\mathsf{T}\mathbf{C}^\mathsf{T} = \mathbf{0}$, then γ is always zero. Once $\gamma = 0$ is obtained, then Eq. (25) can be simplified as

$$\mathbf{P}\mathbf{B} = \alpha\mathbf{C}^\mathsf{T} + \beta\mathbf{A}^\mathsf{T}\mathbf{C}^\mathsf{T}. \tag{27}$$

Now, we need to determine both α and β to satisfy these conditions. Here the solutions are $\alpha = 0$ and $\beta = 1$, such that

$$\mathbf{W} = \mathbf{s}\mathbf{C}\left(\mathbf{s}\mathbf{I_{2\times 2}} - \mathbf{A}\right)^{-\mathbf{1}}\mathbf{B} \tag{28}$$

is a positive real matrix. It holds as long as both $\mathrm{D_1}$ and $\mathrm{D_2}$ are not negative constants. In any event, the value of the damping constants is small such as $\epsilon > 0$, hence the requirement is met. The Lyapunov function in quadratic form is then considered plus an integral of nonlinearity such as

$$\mathcal{V}\left(x\right) = \mathbf{x}^\mathsf{T}\mathbf{P}\mathbf{x} + \mathbf{2}\int_{\mathbf{0}}^{\sigma} \mathbf{f}\left(\sigma\right)\beta\, d\sigma. \tag{29}$$

It is necessary to determine $\mathbf{P}$ to obtain a positive definite Lyapunov function. For ease of analysis, let us partition $\mathbf{P}$ such as

$$\mathbf{P} = \left[\begin{array}{c|c} \mathbf{P_A} & \mathbf{P_B^\mathsf{T}} \\ \hline \mathbf{P_B} & \mathbf{P_C} \end{array}\right] \tag{30}$$

where $\mathbf{P_A}$, $\mathbf{P_B}$, and $\mathbf{P_C}$ are 2×2 submatrices. Simple matrix multiplications, such as

$$\mathbf{P_A}\mathbf{M}^{-\mathbf{1}}\mathbf{K} = \mathbf{K} \tag{31}$$

$$\mathbf{P_B}\mathbf{M}^{-\mathbf{1}}\mathbf{K} = \mathbf{Z_{2\times 1}} \tag{32}$$

are equivalent to the condition in Eq. (27). Since $\mathbf{L}$ is an auxiliary square matrix, $-\mathbf{L}\mathbf{L}^\mathsf{T}$ cannot be a positive definite matrix. Accordingly, Eq. (24) needs to be a negative semidefinite matrix, such that

$$\mathbf{P}\mathbf{A} + \mathbf{A}^\mathsf{T}\mathbf{P} = \begin{bmatrix} \mathbf{P_1} & \mathbf{P_2} \\ \mathbf{P_3} & \mathbf{Z_{2\times 2}} \end{bmatrix} \tag{33}$$

where the submatrices are

$$\mathbf{P_1} = \mathbf{P}_\mathrm{B} + \mathbf{P}_\mathrm{B}^\mathsf{T} - \left(\mathbf{P}_\mathrm{A}\mathbf{M^{-1}D} + \mathbf{DM^{-1}P}_\mathrm{A}\right) \quad (34)$$

$$\mathbf{P_2} = \mathbf{P}_\mathrm{C} - \mathbf{DM^{-1}P}_\mathrm{B}^\mathsf{T} \quad (35)$$

$$\mathbf{P_3} = \mathbf{P}_\mathrm{C} - \mathbf{P}_\mathrm{B}\mathbf{M^{-1}D}. \quad (36)$$

Intentionally, some algebraic operations are performed on Eq. (31), therefore

$$\left(\mathbf{P}_\mathrm{A}\mathbf{M^{-1}} - \mathbf{I_{2\times 2}}\right)\mathbf{K} = \mathbf{Z_{2\times 1}} \quad (37)$$

$$\mathbf{HK} = \mathbf{Z_{2\times 1}} \quad (38)$$

where $\mathbf{H} = \mathbf{M^{-1}P}_\mathrm{A}\mathbf{M^{-1}} - \mathbf{M^{-1}}$ represents a symmetric matrix. According to Eq. (38), the elements of $\mathbf{H}$ must be equal, therefore if we multiply $\mathbf{H}$ with $\mathbf{K}$, it yields the vector $\mathbf{Z_{2\times 1}}$.

Accordingly, $\mathbf{H}$ can be defined as

$$\mathbf{H} = \eta\mathbf{O} \quad (39)$$

to satisfy Eq. (38). Here, η can be any scalar constant, meanwhile, $\mathbf{O}$ is the 2×2 matrix whereby all of its elements are one. $\mathbf{P}_\mathrm{A}$ can then be determined as

$$\begin{aligned}\mathbf{M^{-1}P}_\mathrm{A}\mathbf{M^{-1}} - \mathbf{M^{-1}} &= \eta\mathbf{O}\\ \mathbf{M^{-1}P}_\mathrm{A}\mathbf{M^{-1}} &= \eta\mathbf{O} + \mathbf{M^{-1}}\\ \mathbf{P}_\mathrm{A} &= \eta\mathbf{MOM} + \mathbf{M}. \end{aligned} \quad (40)$$

Now, let η_0 be a scalar which is the solution of

$$\eta_0 = -\left(\mathrm{M}_1 + \mathrm{M}_2\right)^{-1} \quad (41)$$

and $\mathbf{P}_\mathrm{A}$ can be made a positive definite if $\eta > \eta_0$.

Referring to Eq. (33), where $\mathbf{PA} + \mathbf{A}^\mathsf{T}\mathbf{P}$ must be a negative semidefinite matrix. It can be satisfied as long as

$$\mathbf{Q}\left(\eta\right) = -\mathbf{2D} - \eta\left(\mathbf{MOD} + \mathbf{DOM}\right) \quad (42)$$

is a negative semidefinite matrix. Assuming η_1 is the smallest constant that meets the condition, then

$$\det\{\mathbf{Q}\left(\eta_\mathbf{1}\right)\} = \det\{-\mathbf{2D} - \eta_\mathbf{1}\left(\mathbf{MOD} + \mathbf{DOM}\right)\} = \mathbf{0} \quad (43)$$

where det is the determinant of a matrix. It implies that $\mathbf{Q}\left(\eta\right)$ can be a negative semidefinite matrix only if $\eta_1 \leq \eta \leq 0$. Indeed, if $\eta = 0$, then $\mathbf{Q}\left(\mathbf{0}\right) = -\mathbf{2D}$ can be a negative definite matrix.

$\mathbf{PA} + \mathbf{A}^\mathsf{T}\mathbf{P}$ can be guaranteed as a negative semidefinite as long as P2 and P3 are zero submatrices. This can be achieved by asserting

$$\mathbf{P}_\mathrm{C} = \mathbf{P}_\mathrm{B}\mathbf{M^{-1}D} = \mathbf{DM^{-1}P}_\mathrm{B}^\mathsf{T}. \quad (44)$$

Furthermore, from Eqs. (32) and (44), it can be concluded that

$$\mathbf{D^{-1}P}_\mathrm{C}\mathbf{D^{-1}K} = \mathbf{Z_{2\times 1}} \quad (45)$$

$$\mathbf{P}_\mathrm{B} = \eta\mathbf{DOM} \quad (46)$$

$$\mathbf{P}_\mathrm{C} = -\eta\mathbf{DOD}. \quad (47)$$

Let us substitute $\mathbf{P}_\mathrm{A}$, $\mathbf{P}_\mathrm{B}$, and $\mathbf{P}_\mathrm{C}$ from Eqs. (40), (46), and (47) into Eq. (30). $\mathbf{P}$ can then be denoted as

$$\mathbf{P} = \begin{bmatrix} \eta\mathbf{MOM} + \mathbf{M} & \left(\eta\mathbf{DOM}\right)^\mathsf{T} \\ \eta\mathbf{DOM} & -\eta\mathbf{DOD} \end{bmatrix} \quad (48)$$

which is a positive definite matrix.

3.1.1 System with Nonuniform Damping Torques

The Lyapunov function in Eq. (29) can be elaborated further by expanding the quadratic part such that

$$\mathcal{V}\left(x\right) = \boldsymbol{\omega}^\mathsf{T}\mathbf{M}\boldsymbol{\omega} + \eta\boldsymbol{\omega}^\mathsf{T}\mathbf{MOM}\boldsymbol{\omega} + \mathbf{2}\int_\mathbf{0}^\sigma \mathbf{f}\left(\sigma\right)\beta\, d\sigma \quad (49)$$

while its derivative is

$$\dot{\mathcal{V}}\left(x\right) = \boldsymbol{\omega}^\mathsf{T}\mathbf{Q}\left(\eta\right)\boldsymbol{\omega} - \mathbf{2}\left(\boldsymbol{\omega}^\mathsf{T}\mathbf{D}\boldsymbol{\omega} + \eta\boldsymbol{\omega}^\mathsf{T}\mathbf{MOD}\boldsymbol{\omega}\right). \quad (50)$$

If it holds the condition such as

$$0 \geq \eta \geq \max\left(\eta_0, \eta_1\right) \quad (51)$$

then $\mathcal{V}\left(x\right)$ in Eq. (49) is a valid Lyapunov function. It should be noted that the condition in Eq. (51) is a generalization. If the damping constants are not uniform, then η_1 will always be more positive than η_0 [17].

3.1.2 Region of Stability

First, let us assert the relevant theorem regarding the region of stability.

Theorem 1: Indeed, the surface $\mathcal{V}\left(x\right) = \nu \geq 0$. It is assumed that $\sigma_i f\left(\sigma_i\right) \geq 0$ for $i = \{1, 2, \ldots, n-1, n\}$, then the surfaces are bounded for any ν. Let $\nu = \nu_{\max}$ be the smallest nonzero of ν that satisfies

$$\frac{\partial\mathcal{V}\left(\S\right)}{\partial\delta_i} = 0 \quad (52)$$

$$\frac{\partial\mathcal{V}\left(\S\right)}{\partial\omega_i} = 0. \quad (53)$$

Since there is a solution for the surface $\mathcal{V}\left(x\right) = \nu$, a domain also exists containing the origin, enclosed by a surface $\mathcal{V}\left(x\right) = \nu_{\max}$ that belongs to the region of attraction [17].

The solutions in Eq. (52) are the equilibrium load angles, while Eq. (53) indicates that all the angular speeds are equal to zero, such as $\omega_1 = \omega_2 = \cdots =$

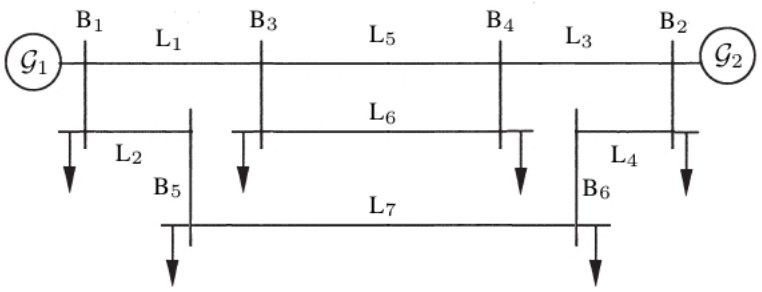

Fig. 3: *Single-line diagram.*

Table 2: *Line information.*

Lines	Buses	Impedances
L_1	B_1–B_3	$0.10 + 0.15i$ pu
L_2	B_1–B_5	$0.25 + 0.25i$ pu
L_3	B_2–B_4	$0.15 + 0.10i$ pu
L_4	B_2–B_6	$0.20 + 0.20i$ pu
L_5	B_3–B_4	$0.15 + 0.05i$ pu
L_6	B_3–B_4	$0.15 + 0.05i$ pu
L_7	B_5–B_6	$0.05 + 0.20i$ pu

$\omega_n = 0$. It can be asserted that the region of stability containing the origin is bounded by

$$\mathcal{V}(x) = \mathcal{V}(x^u) \tag{54}$$

where x^u is the nearest equilibrium state to be necessarily unstable since it contains the origin and $\dot{\mathcal{V}}(x) = 0$ exists, then asymptotic stability can be achieved [16]. The asymptotic stability region can be denoted as

$$\boldsymbol{\omega}^{\mathsf{T}}\mathbf{M}\boldsymbol{\omega} + \eta_1 \boldsymbol{\omega}^{\mathsf{T}}\mathbf{MOM}\boldsymbol{\omega} + \mathbf{2}\int_{\sigma^{\mathbf{u}}}^{\sigma} \mathbf{f}(\sigma)\, d\sigma < 0. \tag{55}$$

3.1.3 Numerical Analysis

For convenience, let us call the areas Area 1 and Area 2. We can simplify the whole system as a single-line diagram (Fig. 3).

It consists of two machines; $\mathcal{G}_1$ and $\mathcal{G}_2$, located in Areas 1 and 2, respectively. Furthermore, both areas are connected by seven transmission lines. In addition, details of the parameters can be seen in Table 2.

Based on this information, we can determine the reduced admittance matrix as

$$\mathbf{Y}_{\text{red}} = \begin{bmatrix} 2.5366 - 2.4838i & -2.5366 + 2.4838i \\ -2.5366 + 2.4838i & 2.5366 - 2.4838i \end{bmatrix} \tag{56}$$

where $\mathbf{Y}_{\text{red}}$ is 2×2 matrix, with respect to the number of machines. Interestingly, if we only have two machines and follow the reduction method in Section 2, the reduced admittance matrix will always be symmetric.

The parameters of these machines also need to be stated here. The parameters of the machine in Area 1, $\mathcal{G}_1$, are as follows: $\mathrm{M}_1 = 1.1$, $\mathrm{P}_{\mathrm{m}1} = 0.7161$ pu, $\mathrm{E}_1 = 1.0566$ pu, and $\mathrm{D}_1 = 0.725$, while those for the machine in Area 2, $\mathcal{G}_2$, are $\mathrm{M}_2 = 1$, $\mathrm{P}_{\mathrm{m}2} = 1.6298$ pu, $\mathrm{E}_2 = 1.0177$ pu, and $\mathrm{D}_2 = 0.7$. These initial conditions are applied in both cases.

We can determine η_0 and η_1 by solving Eqs. (41) and (43). First, by substituting the constants into Eq. (41), $\eta_0 = -0.4762$, implying that $\mathbf{P}_{\mathrm{A}}$ can be made a positive definite if $\eta > -0.4762$. Unlike η_0, there are two solutions to Eq. (43) for η_1. Nevertheless, $\eta_1 = -0.476$ is the right one. Since the solution needs to be a negative scalar, the other one, namely $\eta_1 = 2132$, does not satisfy the condition. It can ultimately be concluded that η_1 is slightly greater than η_0. Hence, the condition for a valid Lyapunov function with non-uniform damping constants is

$$0 \geq \eta \geq -0.476. \tag{57}$$

It will subsequently be shown that η_0 does not serve $\mathbf{Q}(\eta)$ as a negative semidefinite matrix. In our case, we have $\mathrm{D}_1 = 0.725$ and $\mathrm{D}_2 = 0.7$. Whereas, the inertia constants are $\mathrm{M}_1 = 1.1$ and $\mathrm{M}_2 = 1$. Now, let

$$\kappa_i = \frac{\mathrm{D_i}}{\mathrm{M_i}} \tag{58}$$

be the damping constant of the i^{th} machine relative to its inertia. Therefore, by inserting the damping and inertia constants, it yields $\kappa_1 = 0.659$ and $\kappa_2 = 0.7$.

Since κ_2 is larger than κ_1, the angular speeds can be considered as

$$\frac{\mathrm{D_1 M_2}}{\mathrm{D_2 M_1}}\omega_2 < \omega_1 < \omega_2. \tag{59}$$

Taking these constants into the inequality, we then have $0.9416\ \omega_2 < \omega_1 < \omega_2$. Hence, the negative semidefiniteness of $\mathbf{Q}(\boldsymbol{\eta_0})$ can be verified as

$$\boldsymbol{\omega}^{\mathsf{T}}\mathbf{Q}(\eta_{\mathbf{0}})\,\boldsymbol{\omega} = \mathbf{2}\sum_{\mathbf{i=1}}^{\mathbf{2}} (\omega_{\mathbf{2}} - \omega_{\mathbf{1}})\left(\mathrm{D_i M_1}\omega_2 - \mathrm{D_1 M_i}\omega_1\right). \tag{60}$$

By simply letting $\omega_1 = 0.942$, $\omega_2 = 1$, and substituting all the aforementioned constants, we have $\boldsymbol{\omega}^{\mathsf{T}}\mathbf{Q}(\eta_{\mathbf{0}})\,\boldsymbol{\omega} = \mathbf{0.0155}$.

It appears that $\mathbf{Q}(\eta_0)$ is not a negative semidefinite matrix if the damping constants are not uniform, verifying the statement that $\mathbf{Q}(\mathbf{0})$ is a negative definite matrix and η_1 is larger than η_0. Further details and explanations are provided by Willems [16].

3.2 Loss of Transmission Lines

The demand for electrical power is currently increasing, especially from the domestic and industry sectors [22]. Unfortunately, its generation is limited and as a consequence, the transmission lines are rapidly reaching their stability limits [23].

In this study, faults on transmission lines L_6 and L_7 are expected at 40 s in the simulation, and it takes a considerable time for them to be cleared, while impedances at L_6 and L_7 drastically increase.

This implies that the current is unlikely to flow through them, therefore L_5 is the only transmission line capable of connecting to the network. According to this scenario, the reduced admittance matrix during the fault is as follows

$$\mathbf{Y}_{\text{red}}^{\text{df}} = \begin{bmatrix} 1.6 - 1.2i & -1.6 + 1.2i \\ -1.6 + 1.2i & 1.6 - 1.2i \end{bmatrix}. \tag{61}$$

It should be noted that $\mathbf{Y}_{\text{red}}^{\text{df}}$ is a symmetric matrix, obtained by using the same method as $\mathbf{Y}_{\text{red}}$ in Eq. (56). Despite the faults remaining, the synchronism between δ_1 and δ_2 can be preserved as shown in Fig. 4.

We intentionally assign the fault to occur at 40 s of the simulation, thereby allowing ω_1 and ω_2 to become steady as depicted in Fig. 5.

Since $\overline{Y_{11}} = \overline{Y_{22}}$, the initial conditions of δ_1 and δ_2 are identical. It is also applied to ω_1 and ω_2. Interestingly, after faults occur, ω_1 and ω_2 become steady in a new operating condition. Furthermore, the accelerating powers can be observed in Fig. 6. The accelerating power can be defined simply as

$$P_{ai} = P_{mi} - P_{ei}. \tag{62}$$

Intuitively, due to large disturbances, the system may collapse if P_a turns to a negative value. Nevertheless, P_{a1} and P_{a2} remain at positive values, indicating that the faults are not sufficiently significant to disrupt transient stability.

3.3 Unbalanced Load

Unlike the first scenario, here we reduce the admittance matrix during the fault as

$$\mathbf{Y}_{\text{red}}^{\text{df}} = \begin{bmatrix} 3.8776 - 0.9854i & -1.4385 + 0.7621i \\ -1.4385 + 0.7621i & 1.0122 - 0.8432i \end{bmatrix}. \tag{63}$$

Whereas, the post-fault matrix is denoted as

$$\mathbf{Y}_{\text{red}}^{\text{pf}} = \begin{bmatrix} 1.0162 - 0.5146i & -1.0162 + 0.5146i \\ -1.0162 + 0.5146i & 1.0162 - 0.5146i \end{bmatrix}. \tag{64}$$

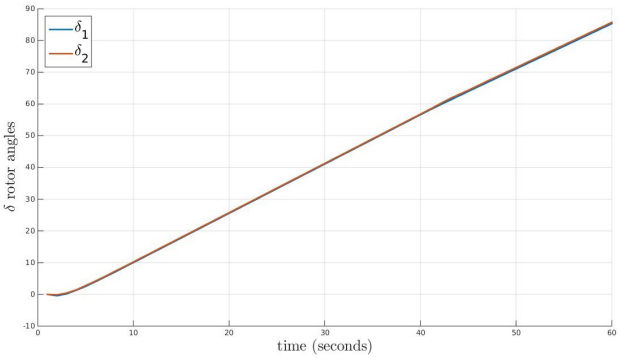

Fig. 4: *First scenario: rotor angles δ_1 and δ_2.*

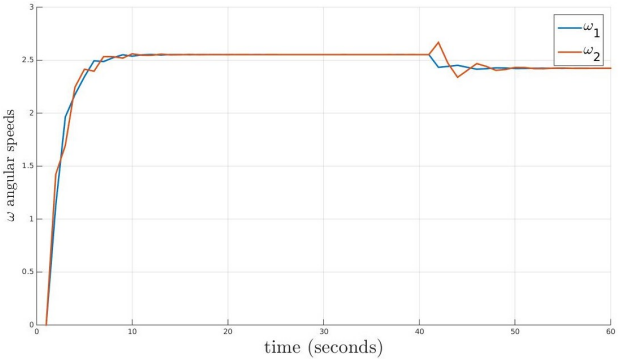

Fig. 5: *First scenario: angular speeds ω_1 and ω_2.*

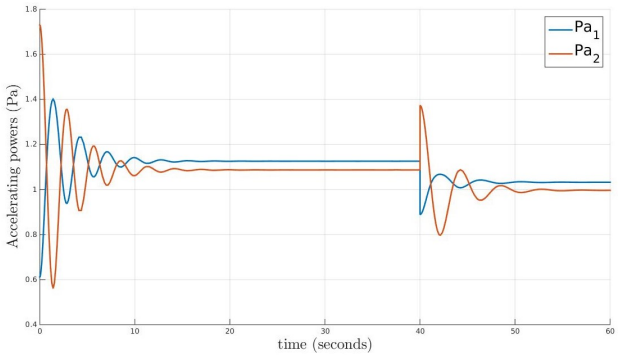

Fig. 6: *First scenario: accelerating powers P_{a1} and P_{a2}.*

Under the earlier assumption that the loads represent constant impedances, it can be implied that the larger conductance G_i yields a greater load at node i^{th}. Whereas, in this scenario, the conductance G_{11}^{df} is larger than G_{22}^{df}.

Initially, the mechanical power input P_{m2} is larger than P_{m1}, yet due to the fault, the electrical power output P_{e1} is larger than P_{e2}, which is why it is referred to as being due to the unbalanced load. This kind of fault may cause rotor angle loss in unison if not cleared. Hence, $\mathbf{Y}_{\text{red}}^{\text{pf}}$ is presented in this scenario.

The post-fault reduced admittance matrix $\mathbf{Y}_{\text{red}}^{\text{pf}}$ is different from $\mathbf{Y}_{\text{red}}$ since most of the time, after the fault is cleared, the operating conditions do not return to their pre-fault condition. Nonetheless, $\overline{Y_{11}^{\text{pf}}} = \overline{Y_{22}^{\text{pf}}}$ is selected, which is similar to the pre-fault condition.

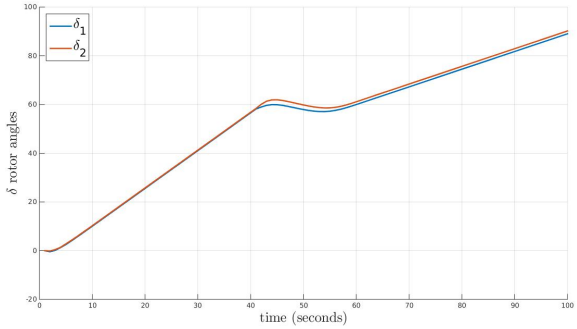

Fig. 7: *Second scenario: rotor angles δ_1 and δ_2 at the CCT.*

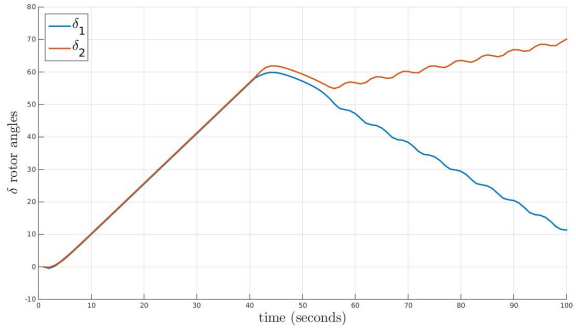

Fig. 10: *Second scenario: rotor angles δ_1 and δ_2 with FCT at 0.4 seconds.*

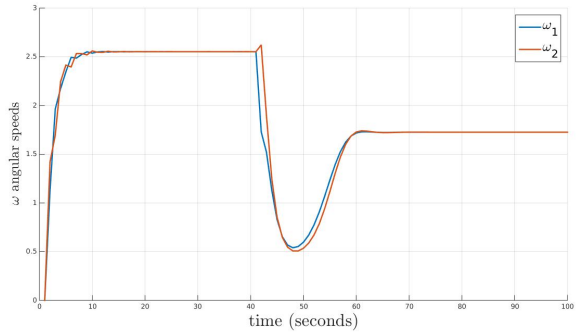

Fig. 8: *Second scenario: angular speeds ω_1 and ω_2 at the CCT.*

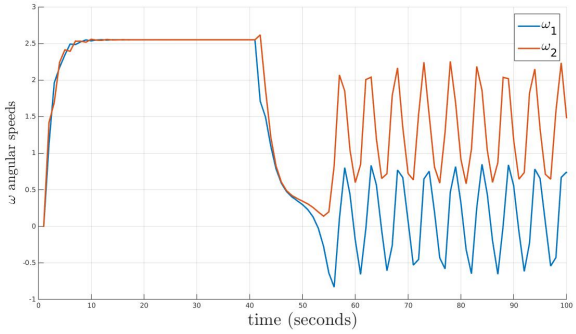

Fig. 11: *Second scenario: angular speeds ω_1 and ω_2 with FCT at 0.4 seconds.*

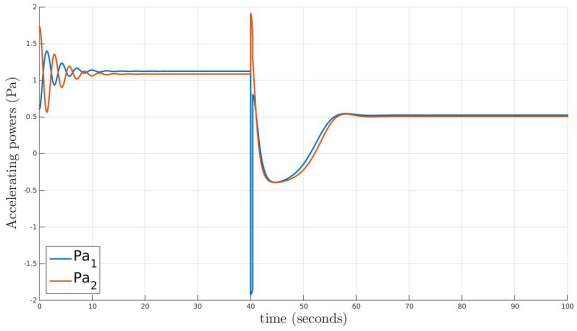

Fig. 9: *Second scenario: accelerating powers $\mathrm{P_{a1}}$ and $\mathrm{P_{a2}}$ at the CCT.*

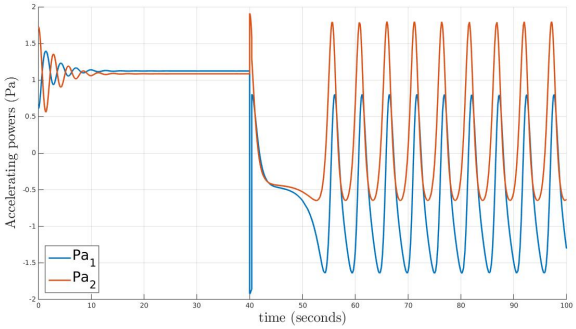

Fig. 12: *Second scenario: accelerating powers $\mathrm{P_{a1}}$ and $\mathrm{P_{a2}}$ with FCT at 0.4 seconds.*

3.3.1 Fault Cleared at CCT

In this section, the simulation is conducted at the point at which the fault is cleared at the CCT. By performing the simulation iteratively, 0.39 s is obtained. In similarity to the first scenario, the fault occurs at 40 s, and is cleared at 40.39 s in simulation time. The fault causes disruption which leads δ_1 to deviate from δ_2.

Eventually, the fault is cleared at the CCT and the rotor angles return, swinging in simultaneity as shown in Fig. 7.

In fact, during the first scenario, even though they are not significant, both ω_1 and ω_2 also deaccelerated, as can be observed from Fig. 8.

The severity of the fault can be depicted by observing the accelerating power in Fig. 9. It can be observed that $\mathrm{P_{a2}}$ declines to the negative level.

3.3.2 Fault Cleared after CCT

In contrast to the previous section, the fault remains after the CCT, being cleared at 40.4 s in simulation time as shown in Figs. 10, 11, and 12.

Since the fault is cleared after the CCT, both δ_1 and δ_2 rotor angles deviate further from each other. Moreover, the fault causes both ω_1 and ω_2 to decelerate, before eventually oscillating separately, as shown in Fig. 11. After the fault occurs, $\mathrm{P_{a1}}$ and $\mathrm{P_{a2}}$ reach a negative level as revealed in Fig. 12, resulting in both accelerating powers being unable to settle into a new operating condition.

4. CONCLUSION

This paper covers the simulation and analysis of multimachine transient stability. It should be noted that the damping constants are not uniform since they affect the stability region. Indeed, there are two simulations here. Firstly, faults due to the loss of transmission lines are investigated and found to be sufficiently significant, and even though they remain, the synchronism can be maintained. Meanwhile, the second scenario introduces the fault due to the load. The fault causes major disruption and needs to be cleared immediately. It must be cleared no more than 0.39 s after occurrence; otherwise, the system becomes unstable. Further analysis is also performed using a Lyapunov function to determine stability. The necessary condition for a valid Lyapunov function is $0 \geq \eta \geq \eta_1$. Based on the numerical computation, the largest stability region can be obtained by assigning $\eta = \eta_1 = -0.476$.

REFERENCES

[1] S. A. Kusumo, Tiyono, and L. M. Putranto, "Transient stability study in grid integrated wind farm," in *2018 5th International Conference on Information Technology, Computer, and Electrical Engineering (ICITACEE)*, Sep. 2018, pp. 61–66.

[2] J. Douglas, "Power system stability and reliability," *IEEE Power Engineering Review*, vol. PER-3, no. 2, pp. 4–7, Feb. 1983.

[3] M. Zainuddin, Sarjiya, T. P. Handayani, W. Sunanda, and F. E. P. Surusa, "Transient stability assessment of large scale grid-connected photovoltaic on transmission system," in *2018 2nd International Conference on Green Energy and Applications (ICGEA)*, 2018, pp. 113–118.

[4] P. Kundur, N. J. Balu, and M. G. Lauby, *Power System Stability and Control*, EPRI power system engineering series. New York, NY, USA: McGraw-Hill Education, 1994.

[5] P. Kundur, J. Paserba, V. Ajjarapu, G. Andersson, A. Bose, C. Canizares, N. Hatziargyriou, D. Hill, A. Stankovic, C. Taylor, T. Van Cutsem, and V. Vittal, "Definition and classification of power system stability," *IEEE Transactions on Power Systems*, vol. 19, no. 3, pp. 1387–1401, Aug. 2004.

[6] G. S. Vassell, "Northeast blackout of 1965," *IEEE Power Engineering Review*, vol. 11, no. 1, pp. 4–8, Jan. 1991.

[7] T. K. Yudhantomo, L. M. Putranto, B. Sugiyantoro, and Tiyono, "Transient stability analysis in grid integrated solar farm," in *2019 5th International Conference on Science and Technology (ICST)*, vol. 1, 2019, pp. 1–6.

[8] T. Hiyama, Y. Fujimoto, and J. Hayashi, "Matlab/Simulink based transient stability simulation of electric power systems," in *1999 IEEE Power Engineering Society Winter Meeting*, vol. 1, Jan. 1999, pp. 249–253.

[9] R. Patel, T. S. Bhatti, and D. P. Kothari, "Matlab/Simulink-based transient stability analysis of a multimachine power system," *The International Journal of Electrical Engineering & Education*, vol. 39, no. 4, pp. 320–336, 2002.

[10] S. Ekinci and A. Demiroren, "Transient stability simulation of multi-machine power systems using Simulink," *Istanbul University - Journal of Electrical and Electronics Engineering*, vol. 15, no. 2, pp. 1937–1944, 2015.

[11] S. Ekinci, H. L. Zeynelgil, and A. Demiroren, "A didactic procedure for transient stability simulation of a multi-machine power system utilizing Simulink," *International Journal of Electrical Engineering Education*, vol. 53, no. 1, pp. 54–71, 2016.

[12] P. W. Sauer and M. A. Pai, *Power System Dynamics and Stability*. Englewood Cliffs, NJ, USA: Prentice-Hall, 1998.

[13] A. Demiroren and H. L. Zeynelgil, "Modelling and simulation of synchronous machine transient analysis using Simulink," *International Journal of Electrical Engineering Education*, vol. 39, no. 4, pp. 337–346, 2002.

[14] M. R. Dadashzadeh and M. Sanaye-Pasand, "A computer software for multimachine power system transient stability analysis," in *39th International Universities Power Engineering Conference, (UPEC 2004)*, vol. 3, Sep. 2004, pp. 1043–1047.

[15] M. A. Pai, *Power System Stability: Analysis by the Direct Method of Lyapunov*, North-Holland systems and control series. Amsterdam, The Netherlands: North-Holland Publishing, 1981.

[16] J. L. Willems, "Optimum Lyapunov functions and stability regions for multimachine power systems," *Proceedings of the Institution of Electrical Engineers*, vol. 117, no. 3, pp. 573–577, March 1970.

[17] J. L. Willems and J. C. Willems, "The application of Lyapunov methods to the computation of transient stability regions for multimachine power systems," *IEEE Transactions on Power Apparatus and Systems*, vol. PAS-89, no. 5, pp. 795–801, May 1970.

[18] H. Kwatny, L. Bahar, and A. Pasrija, "Energy-like Lyapunov functions for power system stability analysis," *IEEE Transactions on Circuits and Systems*, vol. 32, no. 11, pp. 1140–1149, Nov. 1985.

[19] H. K. Khalil, *Nonlinear Systems*, 3rd ed. Englewood Cliffs, NJ, USA: Prentice-Hall, 2002.

[20] J. B. Moore and B. D. O. Anderson, "A generalization of the Popov criterion," *Journal of the Franklin Institute*, vol. 285, no. 6, pp. 488–492, 1968.

[21] B. D. O. Anderson, "A system theory criterion for positive real matrices," *SIAM Journal on Control*, vol. 5, no. 2, pp. 171–182, 1967.

[22] D. Pardi, F. D. Wijaya, and A. I. Cahyadi, "Dynamic modeling of prime mover on microgrid testbed using induction motor inverter drive," in *2019 IEEE 4th International Conference on Technology, Informatics, Management, Engineering Environment (TIME-E)*, 2019, pp. 61–66.

[23] R. Gholizadeh-Roshanagh, B. Mohammadzadeh, and S. Najafi-Ravadanegh, "Optimal siting of UPFC on a transmission line with the aim of better damping of low frequency oscillations," *ECTI Transactions on Electrical Engineering, Electronics, and Communications*, vol. 14, no. 1, pp. 56–64, 2016.

Gilang Nugraha Putu Pratama currently serves as a lecturer in Department of Electronics and Informatics Engineering Education, Universitas Negeri Yogyakarta, Indonesia. He worked as control engineer in Beehive Drones starting from 2019 to 2021. He was also a research assistant in Department of Electrical Engineering, Universitas Gadjah Mada, Indonesia while he co-authored more than 10 papers from 2017 to 2021. Furthermore, recently he has received best paper award in ICITEE 2021. His research interests are robotics and control systems. He is a member of IAENG (International Association of Engineers).

Adha Imam Cahyadi received his bachelor degree from Department of Electrical Engineering, Faculty of Engineering, Universitas Gadjah Mada, Indonesia in 2002, master degree in Control Engineering from King Mongkut's Institute of Technology Ladkrabang, Thailand in 2005, Thailand, and Doctor of Engineering from Tokai University, Japan in 2008. He curently serves as a lecturer in Department of Electrical Engineering and Information Technology, Universitas Gadjah Mada, Indonesia. His research interests are mechanical control systems, telemanipulation systems, and Unmanned Aerial Vehicles. He is a member of IAENG (International Association of Engineers).